ANALYSIS OF THE EFFECTS OF SAIL AND CASING PLACEMENT ON THE HYDRODYNAMIC RESISTANCE OF A U209 SUBMARINE UNDER SUBMERGED CONDITIONS AT VARIOUS SPEEDS USING CFD

Naufal Malik Rafie[1], I Ketut Aria Pria Utama[2]

[1] Department of Naval Architecture, Institut Teknologi Sepuluh Nopember, Surabaya, Indonesia
E-mail: kutama@its.ac.id

Received: August 5, 2026 | **Accepted:** September 25, 2026 | **Published:** September 26, 2026
DOI: 10.12962/j27745449.v6i3.10900 | **Issue:** Volume 6 Number 3 2025 | E-ISSN: 2774-5449

ABSTRACT

This study investigates the effects of casing installation and longitudinal sail position on the hydrodynamic resistance of a fully submerged U209/1300 submarine. Eight configurations were numerically evaluated at speeds of 5, 10, and 15 knots using the Reynolds-averaged Navier–Stokes equations coupled with the shear stress transport turbulence model. The numerical framework was validated against experimental data for the DARPA SUBOFF model, showing a difference of 1.4% in the drag coefficient. The results indicate that the casing increased the total resistance by an average of 8.7% compared with the bare-hull configuration. The combined installation of the sail and casing increased the total resistance by 18.6% to 21.6%. Among the investigated longitudinal positions, the standard sail position consistently produced the lowest resistance, both with and without the casing. The differences in resistance were attributed to variations in wetted surface area, pressure distribution, and hydrodynamic interactions among the hull, sail, and casing. These findings highlight the importance of sail positioning and casing configuration in minimizing the hydrodynamic resistance of fully submerged submarines.

Keyword: Submarine, hydrodynamic resistance, sail position, casing, computational fluid dynamics

Introduction

Submarines play a vital role in modern maritime defense due to their capability to perform surveillance, reconnaissance, and strategic combat missions while remaining submerged. The operational effectiveness of a submarine is strongly influenced by its hydrodynamic performance, which directly affects propulsion power requirements, energy consumption, speed, endurance, and maneuverability [1].

The hydrodynamic resistance of a fully submerged submarine is primarily composed of viscous resistance and pressure resistance. Since wave-making resistance becomes negligible at sufficient submergence depth, the overall resistance is mainly governed by the interaction between the hull geometry and the surrounding flow field [2]. Therefore, optimizing the external geometry of a submarine is essential for improving hydrodynamic efficiency.

Among the external structures affecting submarine resistance, the sail plays an important role in housing operational equipment such as periscopes, antennas, and navigation systems. However, the sail modifies the local pressure distribution and flow development around the hull, potentially generating additional drag. Previous studies have shown that sail geometry and placement significantly influence the hydrodynamic performance of submarines [2,4].

Another important external structure is the casing, which forms the outer contour of the submarine and accommodates various operational systems. Although the casing improves functionality and structural integration, it increases the wetted surface area and may introduce additional flow interference around the hull. Consequently, casing installation generally leads to an increase in hydrodynamic resistance [2-5].

Nasirudin et al. [7] numerically investigated the hydrodynamic resistance characteristics of a modified U209 submarine and reported that casing installation

increased the resistance coefficient by approximately 8% relative to the bare-hull configuration. The addition of a sail further increased resistance due to changes in wetted surface area and flow interaction around the submarine external structures [7].

Although previous studies have investigated the individual effects of sail and casing installations, research concerning the combined influence of casing installation and longitudinal sail-position variations on the hydrodynamic resistance of the U209/1300 submarine remains limited. Therefore, this study aims to investigate the effects of casing installation and sail-position variation on the hydrodynamic resistance of a fully submerged U209/1300 submarine using Computational Fluid Dynamics (CFD). The analysis focuses on total resistance, drag coefficient, resistance components, and flow characteristics to determine the configuration that provides the most favorable hydrodynamic performance.

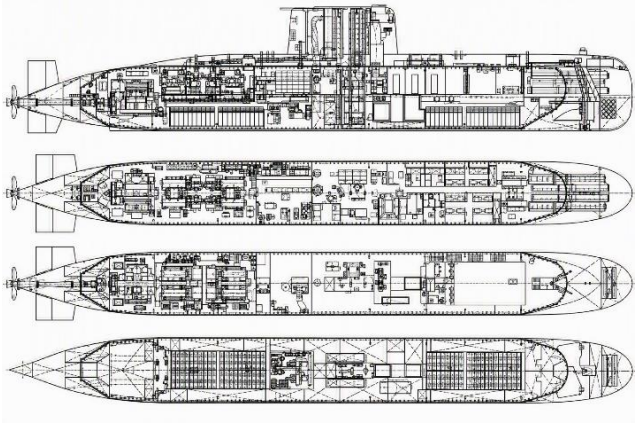


Figure 1. General arrangement of the U209/1300 submarine showing the relationship among the pressure hull, casing, sail, and internal systems [6]

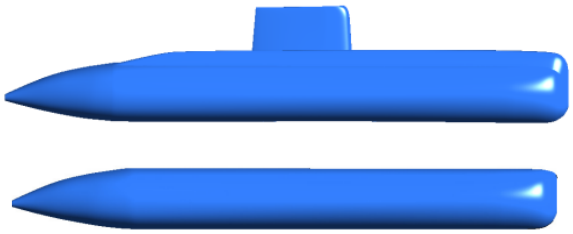


Figure 2. Comparison of the modified U209 configurations with and without a sail and casing

Methodology

Submarine Geometry and Configurations

The DARPA SUBOFF model was employed to verify and validate the numerical framework. The model geometry and experimental resistance data were obtained from published references [12], following the established validation procedure [13]. The principal particulars of the reconstructed DARPA SUBOFF model are presented in Table 1. The validated numerical settings were subsequently applied to all U209/1300 configurations.

Table 1. Comparison of the principal characteristics of the experimental and CFD DARPA SUBOFF models

Symbol	Experiment Model	CFD Model	Unit
L_{pp}	4.356	4.356	m
L/D	8.575	8.575	–
T/D	0.863	0.863	–
L_{FB}/L	0.233	0.233	–
L_{PMB}/L	0.512	0.512	–
L_{AB}/L	0.255	0.255	–
L_{FC}/L	0.210	0.210	–
S_w	6.160	6.163	m²
S_{ws}	0.184	0.187	m²
Δ_{sub}	0.703	0.705	ton

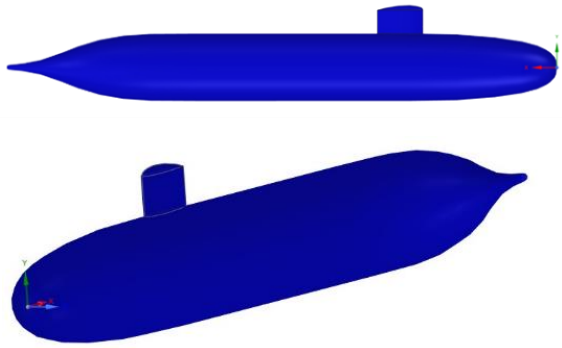


Figure 3. Reconstructed DARPA SUBOFF Geometry

As shown in Table 1, the reconstructed geometry closely matched the experimental model [12]. The differences in wetted surface area and submerged displacement were below 0.5%, confirming that the reconstructed model adequately represented the principal geometric characteristics of DARPA SUBOFF. Following verification and validation, the numerical framework was applied to the U209/1300 Re-Modified geometry. The baseline hull and sail characteristics were derived from published data [13], while the casing arrangement was adapted from a previously developed modified U209 configuration [14]. Eight configurations were investigated to quantify the individual and combined effects of casing presence and longitudinal sail position on hydrodynamic resistance.

Table 2. Investigated U209/1300 configurations.

Model	Casing	L_{FC}/L	S_w(m²)	Δ_{sub}(ton)
BH	No	N/A	1079.891	1634.486
BH-C	Yes	N/A	1166.097	1795.326
SS-STD	No	0.40	1159.891	1673.000
SS-F10	No	0.50	1180.845	1674.000
SS-A10	No	0.30	1180.850	1673.500
SSC-STD	Yes	0.40	1253.910	1835.000
SSC-F10	Yes	0.50	1253.747	1835.520
SSC-A10	Yes	0.30	1254.745	1835.460

Although BH-C and SS-STD have similar wetted surface areas, their external components differ. BH-C includes a casing without a sail, while SS-STD includes the standard sail without casing. The casing adds 86.206 m² to the bare-hull area of 1,079.891 m², whereas the sail adds 80.000 m². Consequently, BH-C is 6.206 m² larger because the casing extends over a greater longitudinal portion of the hull. Only surfaces exposed to the surrounding flow were included in the calculation.

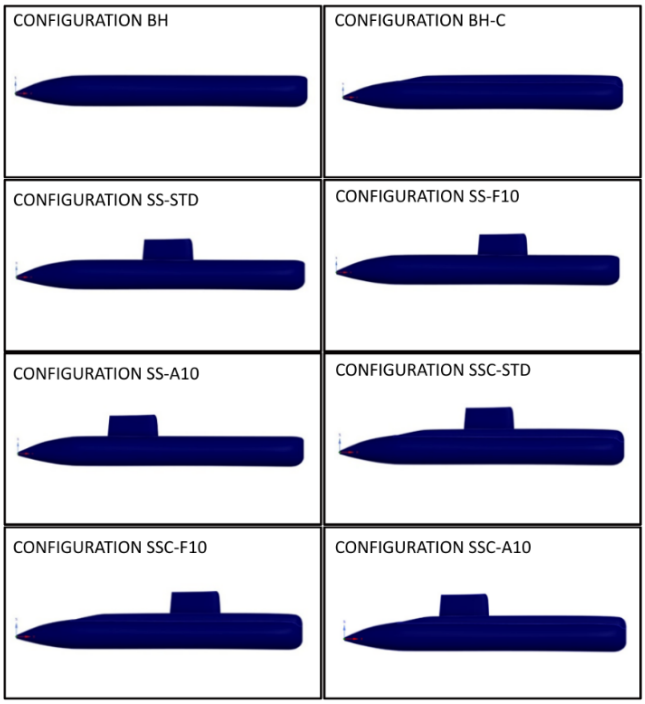


Figure 4. Configurations U209/1300

Computational Domain and Boundary Conditions

A three-dimensional computational domain was constructed to represent the fully submerged operating condition. As shown in Figures 5 and 6, the computational domain had a total longitudinal length of 2L (116.334 m) and a height of 0.75L (43.625 m), where the submarine length L was 58.167 m. The longitudinal domain was divided into 1.5L (87.251 m) and 0.5L (29.084 m) sections. A velocity inlet was specified at the upstream boundary, while a pressure outlet was applied at the downstream boundary. The remaining outer boundaries were defined as walls. These dimensions were selected to provide sufficient clearance for flow development and wake propagation while maintaining a manageable computational cost [13].

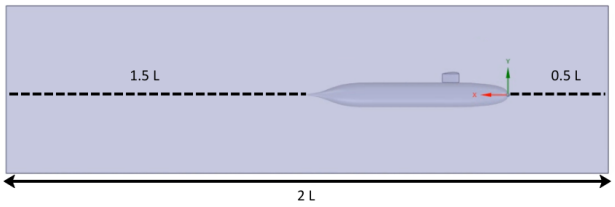


Figure 5. Domain Side View

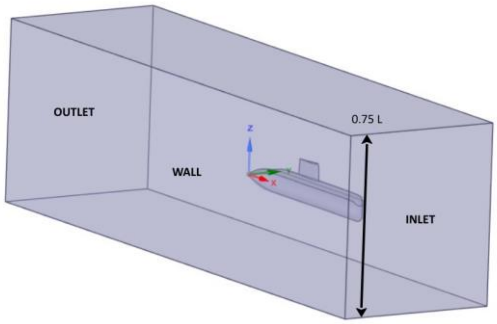


Figure 6. Domain Perspective View

Figure 6 shows the perspective view of the computational domain for the fully submerged simulation. A velocity inlet was applied upstream of the submarine, while a pressure outlet was specified downstream. The surrounding boundaries were defined as walls, and the submarine surface was treated as a stationary no-slip wall. The computational domain dimensions were selected to provide sufficient clearance for inflow and wake development while maintaining a manageable computational cost, following general CFD recommendations [15]. The adequacy of the selected domain was subsequently evaluated based on the converged simulation results.

Mesh Generation and Near-Wall Treatment

A total of 8 inflation layers were applied along the solid-wall boundaries to resolve the near-wall velocity gradients, following established CFD meshing practices [13,15]. A growth ratio of 1.2 and a first-layer thickness of 0.00295 m (2.95 mm) were used to achieve a target y^+ of approximately 1. This configuration enables direct resolution of the viscous sublayer using the k ωSST turbulence model [11,13].

-

The resulting y^+ distribution was evaluated during post-processing because its actual value depends on the local wall shear stress and flow conditions [13,15].

Flow Governing Equations

The flow around the fully submerged submarine was assumed to be steady, incompressible, and turbulent. The governing equations consisted of the conservation of mass and momentum equations. For incompressible flow, the continuity equation is expressed as:

$$\nabla \cdot u = 0 \qquad (1)$$

)

The Reynolds-averaged momentum equation is written as:

$$\rho \bar{u}_j \frac{\partial \bar{u}_i}{\partial x_j} = -\frac{\partial \bar{p}}{\partial x_i} + \mu \frac{\partial^2 \bar{u}_i}{\partial x_j \partial x_j} - \rho \frac{\partial \overline{u_i' u_j'}}{\partial x_j} \qquad (2)$$

where ρ is the fluid density, μ is the dynamic viscosity, $\bar{u}_i$ is the mean velocity component, $\bar{p}$ is the mean pressure, and $-\rho \overline{u_i' u_j'}$ represents the Reynolds stress. Turbulence was modelled using the SST k-ω model, which combines the near-wall capability of the k-ω model with the free-stream characteristics of the k-ε model [11]. The model was selected because of its capability to predict near-wall flow, adverse pressure gradients, and flow separation around the hull, sail, and casing.

Reynolds number and Resistance Equations

The hydrodynamic characteristics of the flow around the submarine were evaluated using the Reynolds number, which represents the ratio between inertial and viscous forces within the fluid flow [21]. The Reynolds number is expressed as:

$$Re = \frac{\rho V L}{\mu} \qquad (3)$$

where Re denotes the Reynolds number, ρ is the fluid density, V is the inflow velocity, L is the characteristic length of the submarine, and μ is the dynamic viscosity.

For a fully submerged submarine, the total hydrodynamic resistance is mainly composed of viscous resistance and pressure resistance [2,21]. Accordingly, the total resistance can be expressed as:

$$R_T = R_V + R_P \qquad (4)$$

where R_T is the total resistance, R_V is the viscous resistance, and R_P is the pressure resistance.

To facilitate the comparison of hydrodynamic performance among the investigated configurations, the drag coefficient was adopted as a dimensionless parameter and calculated as follows:

$$C_D = \frac{R_T}{\frac{1}{2}\rho V^2 S} \qquad (5)$$

where C_D is the drag coefficient, R_T is the total resistance, ρ is the fluid density, V is the free-stream velocity, and S is the wetted surface area [2,21].

Solver Settings

The numerical simulations were performed using a steady, pressure-based solver in ANSYS Fluent. Seawater was modelled as a single-phase incompressible fluid with a density of 1025 kg/m³ and a dynamic viscosity of 0.00105 kg/(m·s). Turbulence was represented using the SST k–ω model because of its capability to resolve near-wall flow and predict adverse pressure gradients and flow separation [11].

Pressure and velocity were coupled using the SIMPLE algorithm [10,15]. Spatial gradients were evaluated using the least-squares cell-based method. First-order upwind discretization was initially applied to obtain a stable solution. After numerical stability was achieved, the discretization schemes for momentum, turbulent kinetic energy, and specific dissipation rate were changed to second-order upwind to improve solution accuracy [10,15].

The under-relaxation factors were set to 0.3 for pressure, 0.7 for momentum, and 0.8 for both turbulent kinetic energy and specific dissipation rate. Convergence was assessed using a residual criterion of 1×10^{-5} and the stability of the monitored drag coefficient. Approximately 2,000 iterations were performed for each simulation. The same numerical settings were consistently applied to the DARPA SUBOFF model and all U209/1300 configurations.

Result and Discussion

Domain Verification

The adequacy of the computational domain was evaluated through the conservation of mass principle. For an incompressible steady-state flow, the inlet and outlet volumetric flow rates should be approximately equal. Therefore, the domain verification was conducted by comparing the volumetric flow rates at the inlet and outlet boundaries [10,15].

$$\varepsilon_Q = \left| \frac{Q_{out} - Q_{in}}{Q_{in}} \right| \times 100\% \qquad (6)$$

where Q_{in} and Q_{out} denote the inlet and outlet volumetric flow rates, respectively.

The computed volumetric flow rates at the inlet and outlet were 5911.7035 m³/s and 5911.8432 m³/s, respectively. Substituting these values into Equation (6) yielded a relative error of only 0.00236%. This very small error indicates satisfactory mass conservation throughout the computational domain and confirms that the selected domain dimensions were sufficiently large to minimize boundary interference effects. Therefore, the computational domain was considered suitable for the subsequent hydrodynamic simulations of the U209/1300 submarine configurations.

Grid Independence and GCI

A grid independence study was performed to evaluate the effect of mesh density on the numerical results. Four mesh levels ranging from 794,182 to 8,839,796 cells were investigated. The variation in drag coefficient continuously decreased as the mesh density increased, indicating mesh convergence. The difference between the medium and fine grids was only 0.16%, demonstrating that the numerical solution had become nearly independent of further mesh refinement [16,17].

The discretization uncertainty was subsequently evaluated using the Grid Convergence Index (GCI) method proposed by Celik et al. [16]. The calculated GCI value was 0.355%, which is significantly lower than the commonly accepted threshold of 1.5%. Therefore, the selected mesh was considered sufficiently accurate for the hydrodynamic analysis of the submarine configurations.

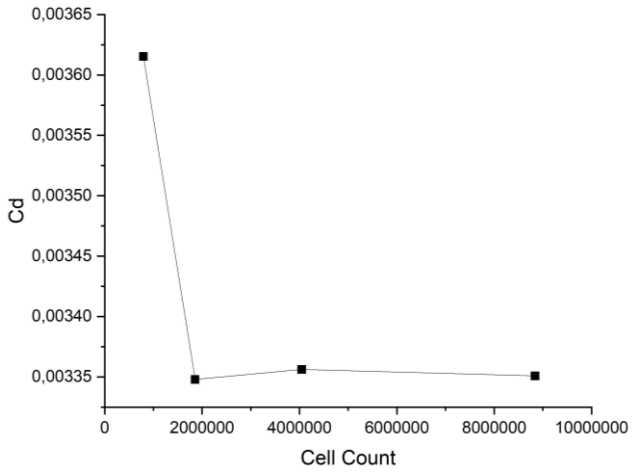


Figure 7. Grid independence study

Darpa Suboff Validation

A comparison between the present CFD prediction, experimental DARPA SUBOFF data, and the numerical results.

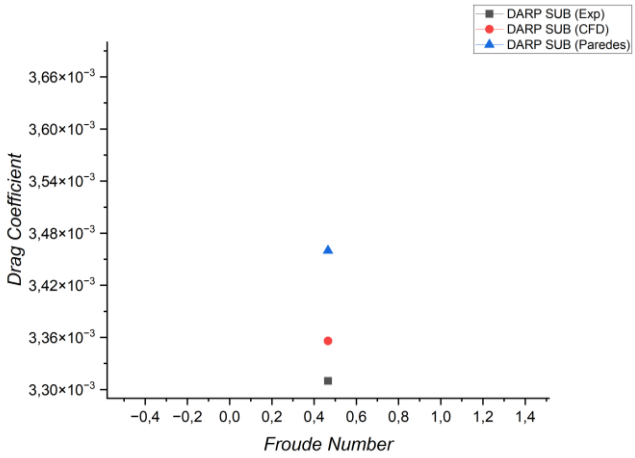


Figure 8. Darpa Suboff Validation Result

Figure 8 compares the drag coefficient predicted by the present CFD model with the experimental DARPA SUBOFF data and the numerical results reported by Paredes et al. [8]. The present simulation yielded a drag coefficient of 0.003356, whereas the experimental value was 0.00331 [12], corresponding to a relative error of approximately 1.4%. This small discrepancy indicates that the numerical setup provides satisfactory accuracy for predicting submarine hydrodynamic resistance. Therefore, the validated CFD framework was subsequently applied to all U209/1300 configurations considered in this study.

Following the verification and validation process, the validated numerical framework was applied to the U209/1300 configurations to investigate the effects of sail position and casing installation on hydrodynamic resistance.

Total Resistance Analysis of the U209/1300 Submarine

As shown in Figure 9, the total resistance increased with increasing operating speed for all configurations. This behavior is expected because the hydrodynamic forces acting on the submarine increase with flow velocity, resulting in higher viscous and pressure resistance components [2,21].

Overall, the results indicate that hydrodynamic resistance increased with operating speed for all investigated U209/1300 configurations. The configurations incorporating both sail and casing (SSC) consistently exhibited the highest total resistance and drag coefficient, whereas the bare-hull (BH) configuration produced the lowest values. Furthermore, viscous resistance was identified as the dominant component, contributing approximately 80-87% of the total resistance. These findings demonstrate that the addition of sail and casing

structures increases the wetted surface area and flow interference around the hull, leading to higher hydrodynamic resistance [2,7,21].

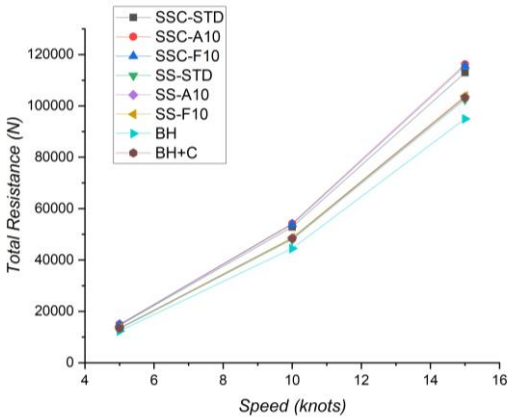


Figure 9. Total resistance of U209/1300 configurations at different operating speeds.

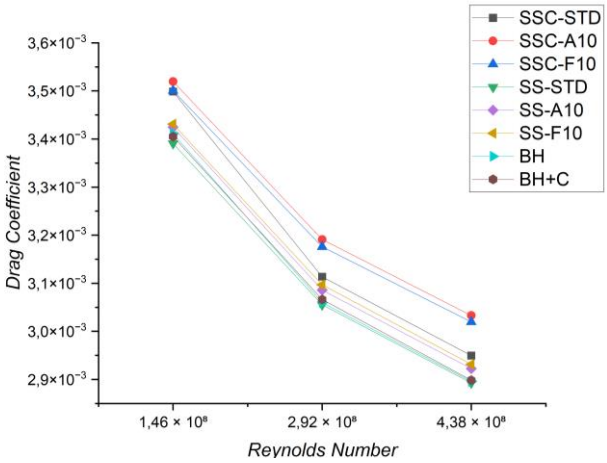


Figure 10. Drag coefficient variation with Reynolds number for all investigated configurations.

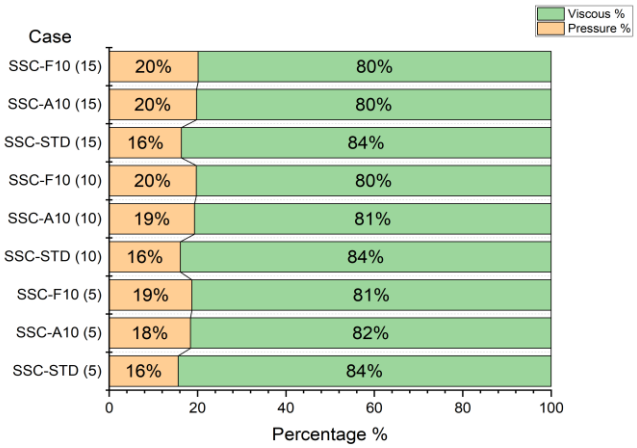


Figure 11. Relative contributions of viscous and pressure resistance to total resistance.

Effect of Sail Position on Hydrodynamic Resistance

The influence of sail position on the hydrodynamic resistance of the U209/1300 submarine was investigated for both configurations without casing (SS) and with casing (SSC). Three longitudinal sail positions were analyzed, namely the standard position (STD), 10%L forward (F10), and 10%L aft (A10). The variation of sail resistance with operating speed is presented in Figures 12 and 13.

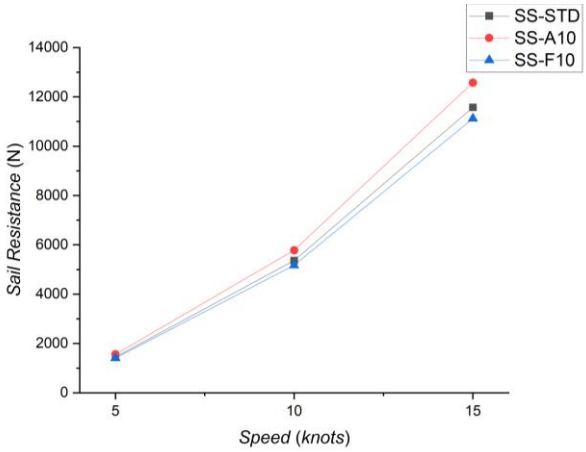


Figure 12. Sail resistance for SS configurations at different operating speeds.

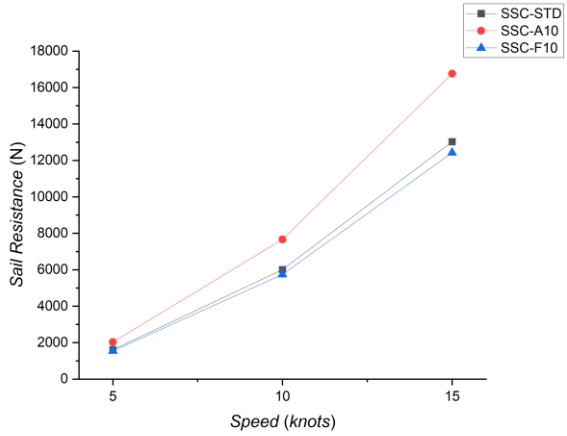


Figure 13. Sail resistance for SSC configurations at different operating speeds.

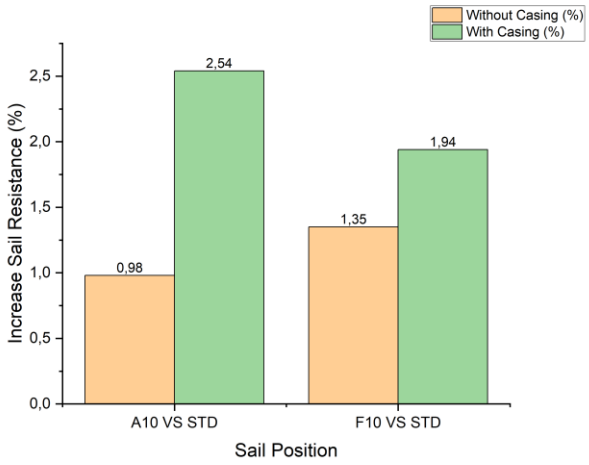


Figure 14. Increase in total resistance due to sail-position variation.

Figures 12 and 13 show that the sail resistance increased substantially with operating speed in both SS and SSC configurations. The A10 position produced the highest sail resistance, reaching approximately 12.58 kN without casing and 16.70 kN with casing at 15 knots, whereas F10 produced the lowest sail-component resistance. However, Figure 14 shows that both sail displacements increased the total resistance relative to STD. Without casing, A10 and F10 increased total resistance by 0.98% and 1.35%, respectively, while with casing, the increases reached 2.54% and 1.94%. This indicates that the casing intensified the hydrodynamic interaction among the sail, casing, and hull, making the standard sail position the most favorable configuration[2,4,7]

Effect of Casing Installation on Hydrodynamic Resistance

The effect of casing installation was evaluated by comparing the submarine configurations with and without casing. The results showed that the presence of the casing consistently increased the total resistance at all investigated speeds.

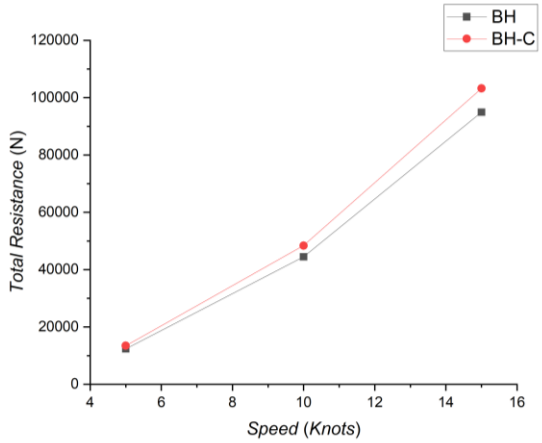


Figure 15. Total resistance of BH and BH-C configurations at different operating speeds.

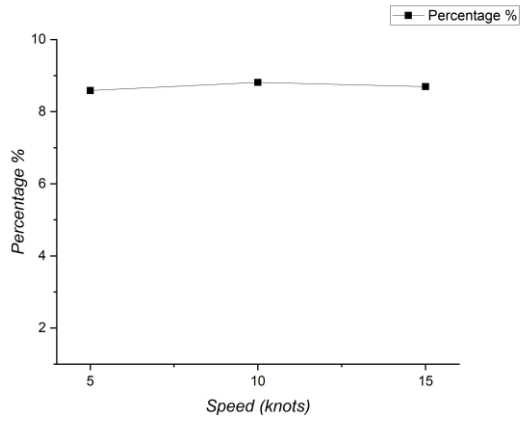


Figure 16. Percentage increase in total resistance due to casing installation.

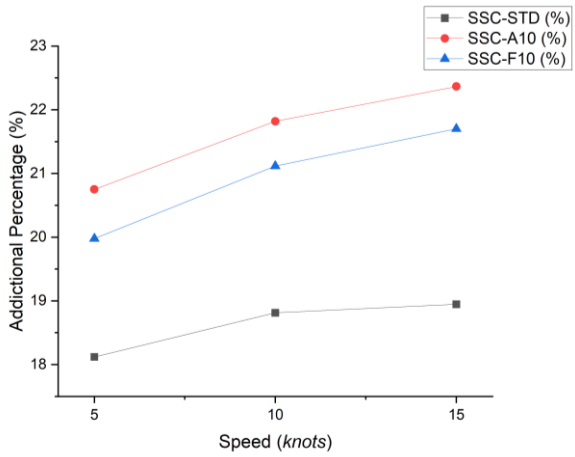


Figure 17. Percentage Increase in Total Resistance Due to Sail and Casing Addition Compared with the Bare Hull (BH) Configuration

The casing increased the total resistance by 8.59%, 8.81%, and 8.70% at 5, 10, and 15 knots, respectively. This increase was primarily caused by the additional wetted surface area [2,7].

The simultaneous addition of the sail and casing increased the total resistance by 18.12–18.95% for SSC-STD, 20.75–22.36% for SSC-A10, and 19.98–21.70% for SSC-F10. SSC-STD consistently produced the lowest increase, indicating that the standard sail position provides the best hydrodynamic performance [7].

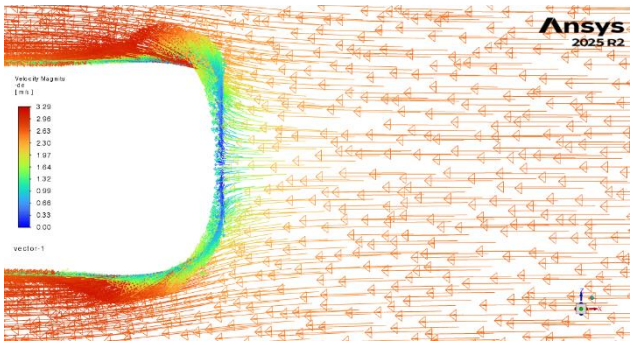


Figure 18. Velocity-vector distribution around the BH (bare-hull) configuration.

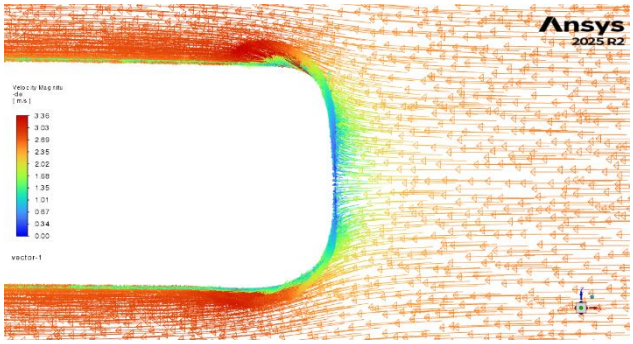


Figure 19. Velocity-vector distribution around the BH-C (bare-hull with casing) configuration.

Physically, the incoming flow decelerates at the bow and forms a stagnation region before accelerating along the hull surface. The addition of the casing changes the upper-hull contour, increases the local velocity gradient, and modifies boundary-layer development. Consequently, the wetted surface area and viscous resistance increase, resulting in higher total resistance for the BH-C configuration than for BH [21].

Conclusion

- The CFD framework was validated against the DARPA SUBOFF experimental data, yielding a drag coefficient error of 1.4% and a Grid Convergence Index of 0.355%.
- Total resistance increased with operating speed, with viscous resistance contributing approximately 80-87% of the total resistance. Casing installation increased total resistance by an average of 8.7% relative to the bare hull.
- Considering the sail component separately, F10 produced the lowest sail resistance, whereas A10 produced the highest. However, relative to STD, A10 and F10 increased total resistance by 0.98% and 1.35% without casing, and by 2.54% and 1.94% with casing, respectively.
- Considering the overall resistance of the hull, sail, and casing, SSC-STD produced the lowest total resistance. The average increases relative to BH were 18.63% for SSC-STD, 20.93% for SSC-F10, and 21.64% for SSC-A10. Therefore, SSC-STD was identified as the most hydrodynamically efficient operational configuration under the investigated conditions.

Acknowledgements

The authors gratefully acknowledge the Department of Naval Architecture, Faculty of Marine Technology, Institut Teknologi Sepuluh Nopember (ITS), for supporting this research. The authors also thank the Hydrodynamics Laboratory for providing the computational facilities and technical resources required for this study.

References

[1] K.J. Rawson, E.C. Tupper, *Basic Ship Theory: Combined Volume*, 5th ed., Butterworth-Heinemann, Oxford, 2001.

[2] M. Renilson, *Submarine Hydrodynamics*, 2nd ed., Springer, Cham, 2018.

[3] K. Dong, X. Wang, D. Zhang, L. Liu, D. Feng, CFD research on the hydrodynamic performance of submarine sailing near the free surface with long-crested waves, *J. Mar. Sci. Eng.* **10** (2022) 90. DOI: 10.3390/jmse10010090.

[4] Sarjito, A. Wijayanto, W.A. Siswanto, Sail position and notch-tail modification to reduce the drag of a mini submarine, *Int. J. Mech. Eng. Technol.* **9** (2018) 515–522.

[5] R.L. Suiker, *Structural Design Tool for a Composite Submarine Non-Pressure Hull*, Master Thesis, Delft University of Technology, 2016.

[6] J. Lee et al., General arrangement and submarine structural configuration of U209/1300, 2008.

[7] A. Nasirudin, Sutiyo, A.N. Yulianto, E. Julianto, I.K.A.P. Utama, M. Renilson, Computational Fluid Dynamics Analysis into the Comparison of Resistance Characteristics Between DARPA Suboff and Modified U209 Types of Submarines, *Sci.* **7** (2025) 82. DOI: 10.3390/sci7020082.

[8] R.J. Paredes, M.T. Quintuña, M. Arias-Hidalgo, R. Datla, Numerical flow characterization around a Type 209 submarine using OpenFOAM, *Fluids* **6** (2021) 66. DOI: 10.3390/fluids6020066.

[9] D. Jung, S. Park, CFD study of submarine hydrodynamics near the free surface in snorkel conditions, *Water* **17** (2025) 734. DOI: 10.3390/w17050734.

[10] F. Moukalled, L. Mangani, M. Darwish, *The Finite Volume Method in Computational Fluid Dynamics: An Advanced Introduction with OpenFOAM and Matlab*, Springer, 2016.

[11] F.R. Menter, Two-equation eddy-viscosity turbulence models for engineering applications, *AIAA J.* **32** (1994) 1598–1605. DOI: 10.2514/3.12149.

[12] H.L. Liu, T.T. Huang, *Summary of DARPA SUBOFF Experimental Program Data*, Naval Surface Warfare Center, Carderock Division, 1998.

[13] ITTC, *Practical Guidelines for Ship Resistance CFD*, Recommended Procedures and Guidelines 7.5-03-02-04, International Towing Tank Conference, 2024.

[14] V. Bertram, *Practical Ship Hydrodynamics*, 2nd ed., Butterworth-Heinemann, Oxford, 2012.

[15] H.K. Versteeg, W. Malalasekera, *An Introduction to Computational Fluid Dynamics: The Finite Volume Method*, 2nd ed., Pearson Education, 2007.

[16] I.B. Celik, U. Ghia, P.J. Roache, C.J. Freitas, H. Coleman, P.E. Raad, Procedure for estimation and reporting of uncertainty due to discretization in CFD applications, *J. Fluids Eng.* **130** (2008) 078001. DOI: 10.1115/1.2960953.

[17] P.J. Roache, *Verification and Validation in Computational Science and Engineering*, Hermosa Publishers, 1998.

[18] A.F. Molland, S.R. Turnock, D.A. Hudson, *Ship Resistance and Propulsion: Practical Estimation of Propulsive Power*, Cambridge University Press, 2011.

[19] E.R. De Fretes, E.B. Djatmiko, W. Wardhana, Hydrodynamic analysis of additional effect of submarine appendages, *Adv. Appl. Fluid Mech.* **13** (2013) 65–74.

[20] A.W. Purwanto, D. Chrismianto, E.S. Hadi, Analisa pengaruh variasi hullform terhadap hambatan total kapal selam dengan metode Computational Fluid Dynamic (CFD), *J. Tek. Perkapalan* **2** (2014).

[21] F.M. White, *Fluid Mechanics*, 4th ed., McGraw-Hill, 1999.